Isolation and Characterization of Copper Methylene ($CuCH_2$) via FTIR Matrix Isolation Spectroscopy

Sou-Chan Chang, Zakya H. Kafafi,‡ Robert H. Hauge, W. Edward Billups,* and John L. Margrave*

Contribution from the Department of Chemistry and Rice Quantum Institute, Rice University, Houston, Texas 77251. *Received September 12, 1986. Revised Manuscript Received February 24, 1987*

Abstract: The reactions of copper atoms with diazomethane in argon and nitrogen matrices at 12 K have been investigated. Fourier transform infrared studies show that copper atoms insert spontaneously into the CN bond of diazomethane in argon matrices to form unligated copper methylene, $CuCH_2$, and dinitrogen coordinated copper methylene, N_2CuCH_2. These two products are found to be photoconvertible; the coordinated N_2 group can be photodissociated with $\lambda \geq 400$ nm photolysis and photoassociated with UV photolysis. A similar insertion reaction also occurs in nitrogen matrices; however, only N_2CuCH_2 is observed and the coordinated N_2 group cannot be photodissociated. Copper–diazomethane complexes, $Cu(CH_2N_2)$, are found in both argon and nitrogen matrices. Photolyses ($\lambda \geq 500$ nm/Ar, $\lambda \geq 420$ nm/N_2) of these $Cu(CH_2N_2)$ adducts lead to the insertion products.

The role of transition metal–carbene complexes as major intermediates in catalytic processes such as alkane activation and olefin metathesis is now well recognized.[1] In a number of other cases, carbene complexes have been invoked but not confirmed. For example, several studies[2] suggest a carbene complex in the copper-catalyzed decomposition of diazo compounds as proposed originally by Yates,[3] but no spectroscopic evidence for these species has, to the best of our knowledge, been reported. Recently, matrix isolation studies of the reactions of the first-row transition metals with diazomethane have been initiated in our laboratory. We have found that iron atoms react spontaneously with diazomethane in argon and nitrogen matrices leading to the matrix isolation and characterization of the simple unligated species $FeCH_2$.[4] In this paper we report the isolation and characterization of the simple unligated species $CuCH_2$ along with the complexes $(N_2)CuCH_2$ and $Cu(N_2CH_2)$ in argon and nitrogen matrices.

Experimental Section

A complete description of the multisurface matrix isolation apparatus has been reported.[5] Copper (Fisher, 99.97%) was vaporized from an alumina crucible enclosed in a tantalum furnace. The furnace was resistively heated over the range 1050–1250 °C, and the temperature was measured with a microoptical pyrometer (Pyrometer Instrument Co.). Diazomethane was prepared from the acyl cleavage of *N*-methyl-*N*-nitroso-*p*-toluenesulfonamide (Aldrich, diazald, 99%).[6] A solution of *N*-methyl-*N*-nitroso-*p*-toluenesulfonamide (0.5 g) in 2-butoxyethanol (2.5 mL) (Aldrich, 99%) was dropped into a solution of 2-butoxyethanol (0.5 mL), H_2O (1.5 mL), and KOH (0.3 g); the mixture was kept under N_2 and stirred magnetically for 10 min at room temperature. Diazomethane was then trapped at 77 K and purified by distillation in vacuo. The portion collected between −110 and −130 °C was used. Deuterated and partially deuterated diazomethane were similarly prepared using 2-butoxyethanol-*d* (75 atom % D), NaOD, and D_2O. Carbon-13 enriched diazomethane was synthesized from *N*-methyl-[^{13}C]-*N*-nitroso-*p*-toluenesulfonamide (MSD Isotopes, 92.1 atom % ^{13}C).

In a typical experiment, copper atoms and diazomethane were co-condensed with argon (Matheson, 99.9998%) or nitrogen (Matheson, 99.9995%) onto a rhodium-plated copper surface over a period of 30 min. The copper block was maintained at 11–14 K by use of a closed-cycle helium refrigerator (Air Products, Displex Model CSW-202). Prior to deposition, the molar ratio of copper, diazomethane, and matrix gas was measured with a quartz crystal microbalance mounted directly on the cold block. During deposition the rate of effusion of copper was continuously monitored with a water-cooled quartz crystal microbalance situated at the back of the furnace via small holes punched into the back of the crucible and the heating element. In this study the molar ratio of copper to matrix gas was varied from 0 to 15 parts per thousand and the molar ratio of diazomethane to matrix gas was varied from 0 to 10 parts per thousand. After deposition, the infrared spectrum of the matrix isolated species was measured with an IBM IR-98 Fourier transform infrared spectrometer. The frequencies were measured over the range 4000–300 cm^{-1} to an accuracy of ±0.05 cm^{-1}.

Some matrix reactions were carried out in the presence of hydrogen (99.9995%, Air Products) or deuterium (99.99%, Air Products). These experiments usually followed the deposition experiments described above with the molar ratio of copper/diazomethane/argon unchanged. A small amount of hydrogen or deuterium (H_2/Ar = 1–5 mmHg/1000 mmHg) was introduced into the system during the 30-min deposition.

Matrices were usually irradiated subsequent to deposition by exposure to a focused 100-W medium-pressure short-arc Hg lamp. The typical exposure time was 10 min. A water filter with various Corning long-pass cutoff filters and a band filter, 280–360 nm, were used for the wavelength-dependent photolysis experiments.

Results

The infrared spectrum resulting from the matrix-isolated copper/diazomethane reaction in solid argon or nitrogen contains a large number of features. The stoichiometry of the reaction products was determined from copper and diazomethane concentration studies. Product absorptions were correlated with their photobehavior to specific wavelength regions. Isotopic molecular studies were carried out to confirm product and mode assignments.

(a) In Argon Matrices. Figure 1 shows the infrared spectra of a copper concentration study in argon matrices. The CH_2N_2/Ar molar ratio was kept constant at 1.27/100 and the Cu/Ar atomic ratio was varied from 0.0 to 1.41%. The results show that the reactions between copper atoms and diazomethane occurred spontaneously upon deposition. The stoichiometry of copper in the various products was determined by a log–log plot of the intensities of absorptions of selected product bands vs. copper concentration,[7] as depicted in Figure 2. A slope of 0.98 was measured for the 614.0 cm^{-1} "a" peak which suggests the presence of atomic copper in this product. A slope close to 2 was determined for the absorption at 550.8 cm^{-1} "d" indicative of a dicopper product. In general the bands which appeared under dilute copper concentrations were found to be due to monocopper reaction

‡Present address: Naval Research Laboratory, Code 6551, Washington D.C. 20375.

(1) Parshall, G. W. *Homogeneous Catalysis*; Wiley-Interscience: New York, 1980.
(2) (a) Skell, P. S.; Etter, R. M. *Chem. Ind. (London)* **1958**, 624; *Proc. Chem. Soc.* **1961**, 443. (b) Nozaki, H.; Moriuti, S.; Yamabe, M.; Noyori, N. *Tetrahedron Lett.* **1966**, 59. (c) Nozaki, H.; Moriuti, S.; Takaya, H.; Noyori, R. *Tetrahedron* **1968**, *24*, 3655. (d) Moser, W. R. *J. Am. Chem. Soc.* **1969**, *91*, 1135 and references therein.
(3) Yates, P. *J. Am. Chem. Soc.* **1952**, *74*, 5376.
(4) Chang, S.-C.; Kafafi, Z. H.; Hauge, R. H.; Billups, W. E.; Margrave, J. L. *J. Am. Chem. Soc.* **1985**, *107*, 1447. A detailed report of this work is forthcoming.
(5) Hauge, R. H.; Fredin, L.; Kafafi, Z. H.; Margrave, J. L. *Appl. Spectrosc.* **1986**, *40*, 588.
(6) (a) deBoer, T. J.; Backer, H. J. *Org. Syn.* **1956**, *36*, 16. (b) Moore, C. B. *J. Chem. Phys.* **1963**, *39*, 1884.
(7) Moskovits, M.; Ozin, G. A. *Cryochemistry*; Wiley-Interscience: New York, 1976.

0002-7863/87/1509-4508$01.50/0

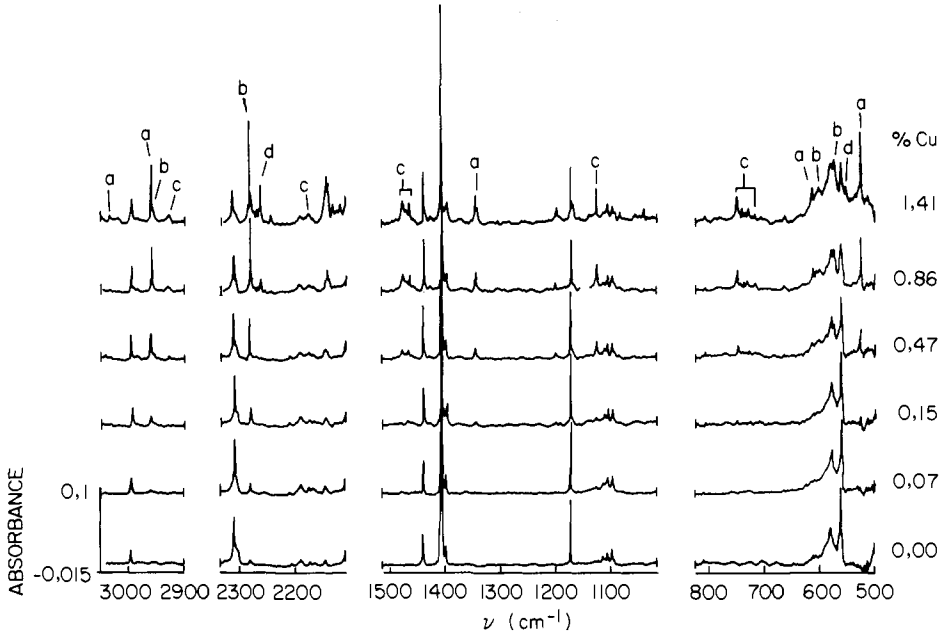

Figure 1. A copper concentration study. $CH_2N_2/Ar \simeq 1.27/100$: (a) $CuCH_2$, (b) N_2CuCH_2, (c) $Cu(CH_2N_2)$, (d) dicopper and copper clusters reaction products.

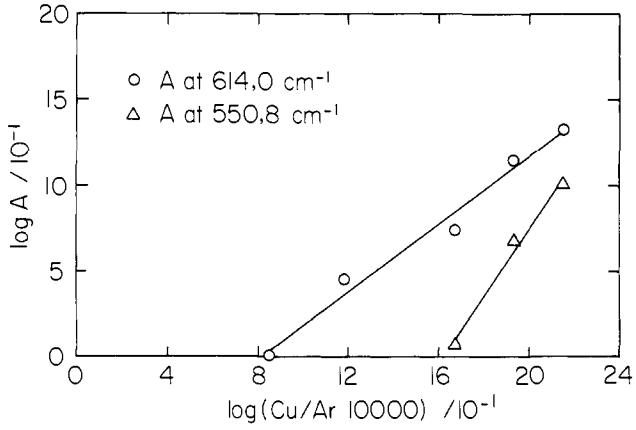

Figure 2. Log A vs. log (Cu/Ar × 10 000) plot. A represents the absorbance; Cu/Ar represents the atomic ratio of copper and argon. The slope of the line at 614.0 cm^{-1} (open circle) is 0.98; at 550.8 cm^{-1} (open triangle) it is 1.95.

products. Some weak absorptions at 2260.4, 1083.8, 1039.4, and 555.2–548.6 cm^{-1} were observed at higher Cu concentrations. These bands are related to dicopper or larger copper cluster products and will not be discussed in the present paper.

Although the infrared spectra of the copper/diazomethane reaction products appeared to be initially fairly complex, the separation of these products was achieved easily by selected wavelength photolysis studies. Figure 3 shows the results of a broad-band photolysis study of a Cu/CH_2N_2 reaction in an argon matrix. The bottom spectrum (Figure 3, A) reflects the absorptions of products derived from reactions of monocopper atoms after deposition. This spectrum was simplified with the disappearance of "c" bands after $\lambda \geq 500$ nm photolysis (Figure 3, B–A). The disappearance of the bands labeled "c" was accompanied by the growth of the bands labeled "a" and "b". No new absorptions associated with copper/diazomethane reaction products were observed.

The "c" bands with frequencies analogous to CH_2N_2 values were assigned to a perturbed diazomethane or better described as a $Cu(CH_2N_2)$ complex. The photolytically enhanced bands, "a"

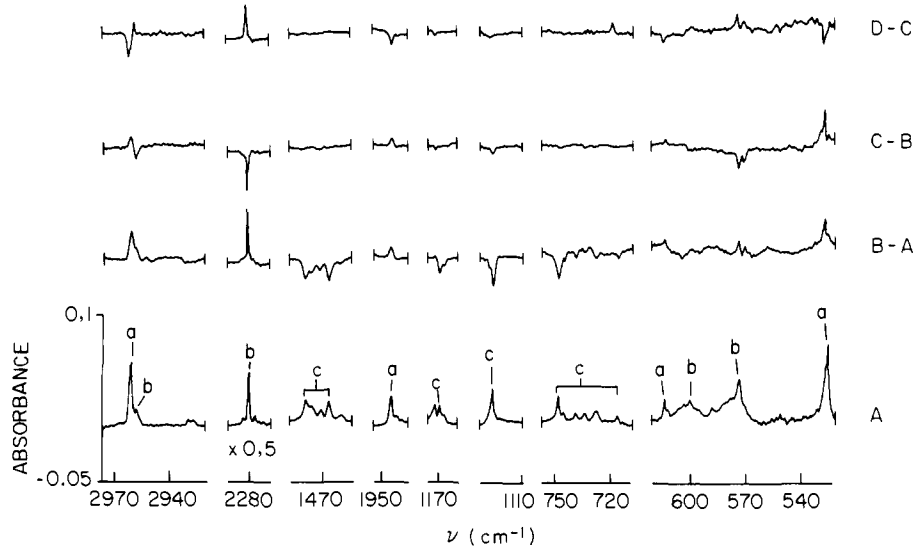

Figure 3. A photolysis study in an argon matrix. $Cu/CH_2N_2/Ar \simeq 0.86/1.27/100$: (A) no photolysis, (B) after 10-min photolysis with $\lambda \geq 500$ nm, (C) after 10-min photolysis with $\lambda \geq 400$ nm, (D) after 10-min photolysis with 380 nm $\geq \lambda \geq 280$ nm; (a) $CuCH_2$, (b) N_2CuCH_2, (c) $Cu(CH_2N_2)$ adducts.

Table I. Measured and Calculated Infrared Frequencies (cm^{-1}) for $CuCH_2$, $Cu^{13}CH_2$, CuCHD, and $CuCD_2$ in Solid Argon

	$CuCH_2$		$Cu^{13}CH_2$		CuCHD		$CuCD_2$	
vibration mode	obsd	calcd	obsd	calcd	obsd	calcd	obsd	calcd
CH_2 s-stretch	2960.7	2961.6	2955.6	2954.8	2219.0	2218.5		2160.4
CH_2 scissor	1344.9	1346.0	1338.6	1339.7	1196.0	1191.8	1013.7	1015.2
CuC stretch	614.0	615.6	597.6	599.4	610.9	609.6	570.4	567.2
CH_2 a-stretch	3034.7	3035.9	3024.1	3022.9	2996.6	2996.7		2263.4
CH_2 rock		573.2		569.9		474.1		433.2
CH_2 wag	526.0	524.8	521.7	520.0	471.0	472.3	409.1	413.0

Table II. Measured and Calculated Infrared Frequencies (cm^{-1}) for N_2CuCH_2, $N_2Cu^{13}CH_2$, N_2CuCHD, and N_2CuCD_2 in Nitrogen and Argon Matrices

		N_2CuCH_2		$N_2Cu^{13}CH_2$		N_2CuCHD		N_2CuCD_2	
vibration mode		obsd	calcd	obsd	calcd	obsd	calcd	obsd	calcd
CH_2	N_2	2943.1	2944.1	2937.5	2936.6		2184.3	2155.3	2155.0
s-stretch	Ar	2957.3		2952.3					
CH_2	N_2	1366.6	1366.8	1360.3	1360.7	1211.6	1211.3	1027.9	1026.9
scissor									
CuC	N_2	613.0	614.8	597.1	598.7	608.2	610.0	572.3	566.7
stretch									
CH_2	N_2	3002.9	3002.3	2992.5	2993.1	2972.3	2972.4		2206.8
a-stretch	Ar					2987.7			
CH_2	N_2	590.6	594.2	586.7	590.1	500.2	493.6	464.3	455.9
rock	Ar	600.3						468.9	
CH_2	N_2	569.1	569.4	564.1	564.1	512.3	512.7	449.8	448.8
wag	Ar	573.5		568.9		515.6		451.5	
N≡N	N_2	2293.7	*a*	2293.7	*a*	2293.7	*a*	2293.7	*a*
stretch	Ar	2279.9		2279.9		2279.7		2279.7	

[a] N≡N stretching frequencies were not calculated.

and "b", were located in mainly four regions: 3100–2900, 2300–2200, 1400–1300, and 700–500 cm^{-1}, which are characteristic of $\nu(CH_2)$ stretching, $\nu(N{\equiv}N)$ stretching, $\delta(CH_2)$ bending, and $\nu(CuC)$ stretching and $\rho_w(CH_2)$ wagging modes, respectively.

Close inspection of the spectrum (Figure 3, A–B) reveals that an increase in the "a" and "b" bands did not occur to the same degree after $\lambda \geq 500$ nm photolysis. The "b" bands at 2957.3, 2279.9, 600.3, and 573.5 cm^{-1} increased by 80%, while the bands at 3034.7, 2960.7, 1344.9, 614.0, and 526.0 cm^{-1} increased by only 30%. The former set was assigned to N_2CuCH_2 because of the strong N≡N stretching absorption at 2279.9 cm^{-1}. The latter set was assigned to $CuCH_2$. A doublet splitting with a 2:1 ratio for the 614 cm^{-1} band indicates that this absorption is due to a CuC stretching mode where only one copper atom is involved (natural abundance of Cu^{65} = 69.1%, Cu^{63} = 30.8%). The photoinsertion products, $CuCH_2$ and N_2CuCH_2, were formed in a 2 to 1 ratio after $\lambda \geq 500$ nm photolysis as compared to a 4 to 1 ratio for reactions upon deposition. The increased amount of N_2CuCH_2 relative to $CuCH_2$ is reflecting the more efficient quenching of the reaction energy by the matrix cage.

Further photolysis studies showed that these two sets of bands were photoreversible. The set assigned to N_2CuCH_2 decreased in intensity after $\lambda \geq 400$ nm photolysis (Figure 3, C–B) but regained intensity after UV photolysis (Figure 3, D–C), while the set assigned to $CuCH_2$ showed the reverse behavior. This photoreversible phenomenon indicates that the coordinated N_2 can be photodissociated with $\lambda \geq 400$ nm photolysis and photoassociated with UV photolysis. These observations suggest that the reaction of copper atom and diazomethane can be described as follows:

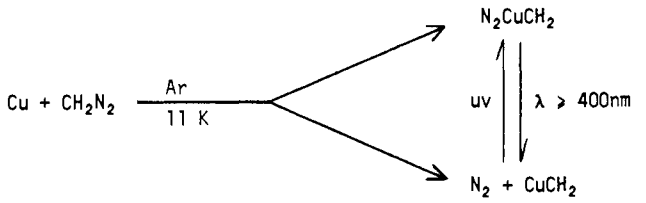

In order to verify and confirm the above assignments, experiments of copper atoms with $^{13}CH_2N_2$, $CHDN_2$, and CD_2N_2 were carried out. Figure 4 shows the absorptions of $CuCH_2$, $Cu^{13}CH_2$, CuCHD, and $CuCD_2$ in argon matrices. The Cu^{65} isotopic shifts were also observed as the doublet splitting or shouldering in a 2:1 ratio at the CuC stretching bands. The vibrational mode assignments for $CuCH_2$ and its isotopic molecules were further supported by a complete normal coordinate analysis. The observed and calculated frequencies are listed in Table I and will be discussed later. Table II shows the measured frequencies for N_2CuCH_2 and its isotopic molecules; except for the N≡N stretching band, all the isotopic frequencies were shifted as expected. The "unshifted" N≡N stretching frequency indicates that there is very little coupling between the nitrogen molecule and the methylene group.

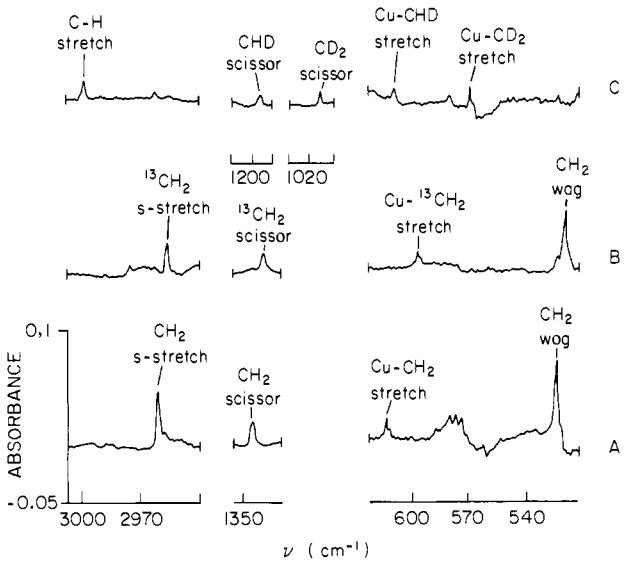

Figure 4. An isotopic study. FTIR spectra of $CuCH_2$ (A), $Cu^{13}CH_2$ (B), CuCHD and $CuCD_2$ (C) in argon matrices.

Adding H_2 or D_2 during the deposition caused a decrease in the insertion product absorptions. No reduction intermediate products of the copper methylene species, such as $HCuCH_3$ or $CuCH_3$,[8] were observed before or after photolysis. Methane was

(8) Parnis, J. M.; Mitchell, S. A.; Garcia-Prieto, J.; Ozin, G. A. *J. Am. Chem. Soc.* **1985**, *107*, 8169.

(9) Wilson, E. B., Jr.; Decius, J. C.; Cross, P. C. *Molecular Vibrations*; McGraw-Hill: New York, 1955, and references therein.

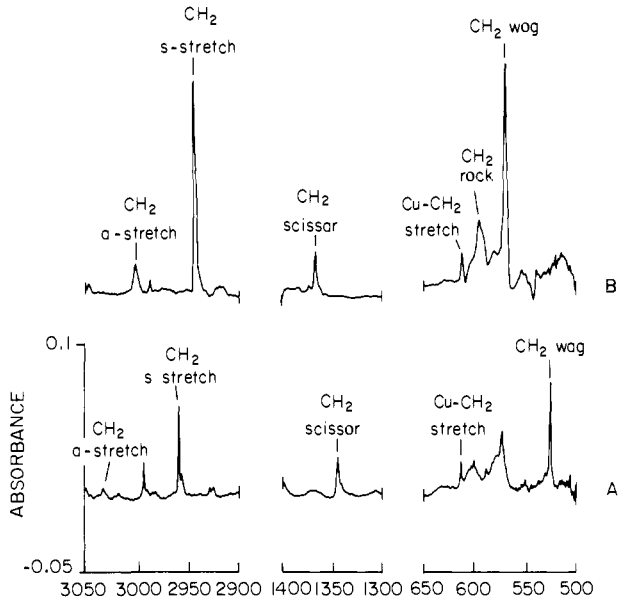

Figure 5. FTIR spectra of $CuCH_2$ in an argon matrix (A) and in a nitrogen matrix (B).

formed after $\lambda \geq 420$ nm photolysis; however, it was found that the same reaction could occur with only hydrogen and diazomethane present, although the production of methane appeared to be enhanced in the presence of copper. Thus it may be that some $CuCH_2$ is reduced to methane.

(b) In Nitrogen Matrices. The reaction of copper atoms and diazomethane in nitrogen matrices was similar to that in Ar matrices; however, most of the frequencies showed a significant matrix shift. Only one insertion product, N_2CuCH_2, was found in nitrogen matrices. This species exhibited absorptions at 3003.1, 2943.1, 2293.7, 1366.6, 613.0, 595.2, 590.8, and 569.1 cm^{-1}. These frequencies are similar to those of N_2CuCH_2 in argon matrices. The coordination of a N_2 group is confirmed by the presence of a N≡N stretching band at 2293.7 cm^{-1}. Reactions using $^{13}CH_2N_2$, $CHDN_2$, and CD_2N_2 have also been carried out in nitrogen matrices to confirm the above assignments. The vibrational mode assignments of the insertion product were further supported by a complete normal coordinate analysis. These results are shown in Table II.

Figure 5 shows the spectra of the main insertion products of the Cu/CH_2N_2 reaction in an argon matrix and in a nitrogen matrix, under approximately the same reaction conditions. Note that the peak intensities of N_2CuCH_2 in the nitrogen matrix (Figure 5B) are stronger than for $CuCH_2$ in an argon matrix (Figure 5A).

The $Cu(CH_2N_2)$ adduct bands were also observed in nitrogen matrices. The photolytic behavior of $Cu(CH_2N_2)$ adducts in nitrogen matrices was somewhat different from that in argon matrices. Irradiation with $\lambda \geq 420$ nm rather than with $\lambda \geq 500$ nm was required for photoinsertion to take place in a nitrogen matrix. Two relatively distinct forms of $Cu(CH_2N_2)$ adducts were found in a nitrogen matrix.

The results of a photolysis study of Cu/CH_2N_2 in a nitrogen matrix are shown in Figure 6. All of the $Cu(CH_2N_2)$ adducts bands labeled "c1" and "c2" disappeared after $\lambda \geq 420$ nm photolysis and led to N_2CuCH_2 labeled "a" (Figure 6, C–B); however, photolysis with $\lambda \geq 500$ nm caused only slight frequency shifts of the initial "c1" adduct bands (Figure 6, B–A). This observation indicates that there are two different adducts formed during deposition. The "c1" bands that shifted slightly (presumably changing matrix sites) after $\lambda \geq 500$ nm photolysis and disappeared after $\lambda \geq 420$ nm photolysis were assigned to adduct A. The "c2" bands that were unaffected upon $\lambda \geq 500$ nm photolysis but disappeared after $\lambda \geq 420$ nm photolysis were assigned to adduct B.

The frequencies and the tentative assignments for the adducts and their isotopic molecules in both argon and nitrogen matrices are listed in Table III.

Table III. FTIR Frequencies (cm^{-1}) for Diazomethane and Copper–Diazomethane Complexes in Argon and Nitrogen Matrices

vibrational mode for free CH_2N_2[a]		$Cu(CH_2N_2)$		$Cu(^{13}CH_2N_2)$		$Cu(CD_2N_2)$	
		Ar	N_2	Ar	N_2	Ar	N_2
CH_2 wag	D	402.1	427.2	397.7	422.8	323.7	337.5
	A	716.4	719.8	716.4	713.5	619.0	621.0
	B	728.5	767.5	722.0	753.3	634.0	
		734.3		727.5		639.3	
		748.7		741.7			
CH_2 scissor	D	1172.3	1169.6	1158.0	1155.9	965.0	965.4
	A	1169.9	1209.5	1161.0	1199.8	994.0	
	B	1126.5	1127.4	1117.3	1119.0	909.5	913.3
C=N stretch	D	1407.8	1406.6	1398.4	1397.2	1213.2	1211.6
	A	1551.5	1571.9	1536.0	1560.9	1500.8	1546.2
			1577.9		1566.0	1510.2	1556.3
	B	1466.1	1486.9	1454.3	1484.0	1226.0	
		1470.7		1469.7		1230.0	
		1475.0		1476.0		1233.3	
N≡N stretch	D	2096.7	2096.5	2096.8	2092.6	2090.5	2091.4
	B	2174.3	2196.8		2195.0		2201.3
CH_2 s-stretch	D	3070.1	3068.4	3065.1	3063.6	2238.2	2236.8
	B	2926.9	2926.0	2922.0			
		2929.8		2925.0			

[a] Reference 14; D = CH_2N_2; A, B = $Cu(CH_2N_2)$.

Table IV. Symmetry Coordinates and Force Constants Used for $CuCH_2$, $Cu^{13}CH_2$, CuCHD, and $CuCD_2$

A′	$S_1 = 2^1/_2(\Delta r_1 + \Delta r_2)$	F_{11} = 4.847 mdyn/Å
	$S_2 = \Delta r_3$	F_{12} = 0.512 mdyn/Å
	$S_3 = 6^1/_2(2\Delta\phi_1 - \Delta\phi_2 - \Delta\phi_3)$	F_{13} = −0.314 mdyn/rad
	$S_4 = 2^1/_2(\Delta r_1 - \Delta r_2)$	F_{22} = 2.659 mdyn/Å
	$S_5 = 2^1/_2(\Delta\phi_2 - \Delta\phi_3)$	F_{23} = −0.018 mdyn/rad
A″	$S_6 = \Delta\theta_1 \sin \phi_1$	F_{33} = 0.397 mdyn Å/rad^2
		F_{44} = 4.868 mdyn/Å
		F_{45} = −0.073 mdyn/rad
		F_{55} = 0.190 mdyn Å/rad^2
		F_{66} = 0.088 mdyn Å/rad^2

Discussion

We have found that in argon matrices copper atoms react with diazomethane spontaneously to form diazomethane–copper adducts $Cu(CH_2N_2)$ and the insertion products, $CuCH_2$ and N_2CuCH_2. A similar reaction also occurs in nitrogen matrices with the formation of N_2CuCH_2 and $Cu(N_2CH_2)$. The insertion of Cu atoms into the CN bond of CH_2N_2 is expected to be exothermic and clearly does occur spontaneously; however, two types of diazomethane–copper adducts are also formed. A photoinsertion reaction occurs for these $Cu(CH_2N_2)$ adducts after irradiation ($\lambda \geq 500$ nm/Ar, $\lambda \geq 420$ nm/N_2) and produces the insertion products. Thus the $Cu(CH_2N_2)$ adducts can be regarded as intermediates of the insertion reaction which are in some way stabilized as a complex by the matrix, possibly as less reactive adducts involving copper atom interaction with only the nitrogen. Possible structures for the $Cu(CH_2N_2)$ adducts are:

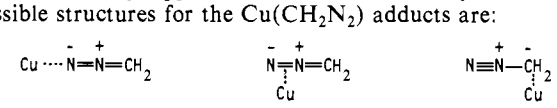

1 2 3

Structures **1** and **2** would be the most likely to be trapped as complexes whereas structure **3** might be expected to proceed directly to the insertion product.

It is interesting to note that the vibrational absorptions of the insertion product in nitrogen matrices are generally similar to N_2CuCH_2 in argon matrices. Thus it seems likely that only one N_2 molecule is significantly interacting with $CuCH_2$ in the nitrogen matrix (note the similarity of the wagging and rocking modes);

(10) (a) Rappe, A. K.; Goddard, W. A., III *J. Am. Chem. Soc.* **1977**, *99*, 3966. (b) Spangler, D.; Wendoloski, J. J.; Dupuis, M.; Chen, M. M. L.; Schaefer, H. F., III *Ibid.* **1981**, *103*, 3985.

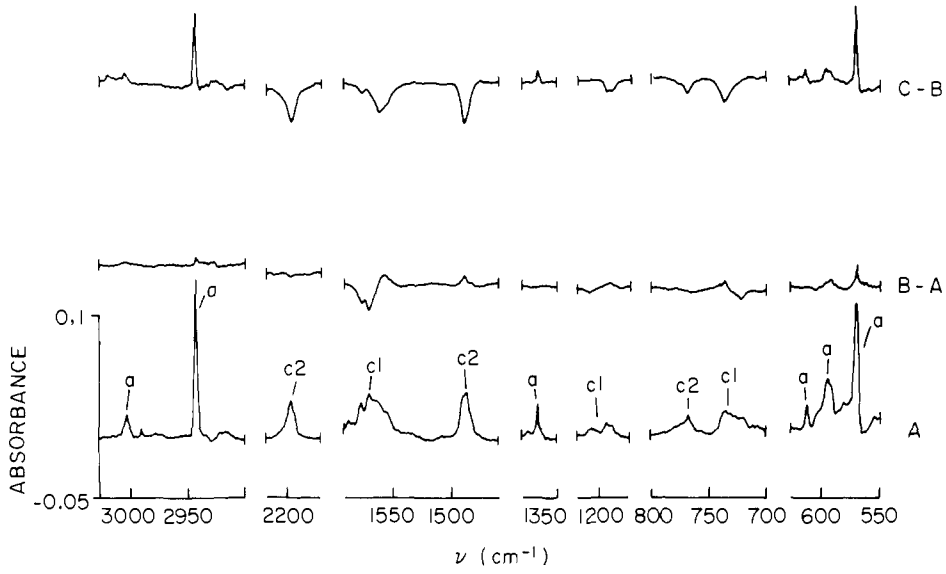

Figure 6. A photolysis study in a nitrogen matrix. $Cu/CH_2N_2/N_2 \simeq 0.83/1.01/100$: (A) no photolysis, (B) after 10-min photolysis with $\lambda \geq 500$ nm, (C) after 10-min photolysis with $\lambda \geq 400$ nm, (D) after 10-min photolysis with 380 nm $\geq \lambda \geq 280$ nm; (a) $CuCH_2$, (c1) $Cu(CH_2N_2)$ adduct A, (c2) $Cu(CH_2N_2)$ adduct B.

however, the intensities of the absorptions arising from N_2CuCH_2 were much stronger in nitrogen matrices, and almost all the fundamental vibrations were observed.

The structure of $CuCH_2$ may have either C_{2v} (planar) or C_s (nonplanar) symmetry. The molecular structure derived from the application of the product and sum rules[9] using the available frequencies favors the C_{2v} planar symmetry. By using the Teller–Redlich product rule for A_1 vibrational species in C_{2v} symmetry the predicted and observed ratios are found to be in good agreement for both $CuCH_2/Cu^{13}CH_2$ (1.034, 1.034) and N_2CuCH_2/N_2CuCD_2 (N_2) (1.973, 1.945). For CuCHD with a planar structure the molecular symmetry becomes C_s with symmetry species A′ corresponding to A_1 and B_1 species of C_{2v} and the A″ species corresponding to B_2 of C_{2v}. The frequencies of CuCHD are simply related to those of $CuCH_2$ and $CuCD_2$ through the isotopic sum rule:

$$2\sigma(CuCHD) = \sigma(CuCH_2) + \sigma(CuCD_2)$$

where $\sigma = 4\pi^2\Sigma_i\nu_i^2$. The result of applying the sum rule to the A′ species (i.e., a value of a calculated frequency of 471.2 cm^{-1} for CuCHD as compared to the observed value of 471.0 cm^{-1}) also indicates that $CuCH_2$ is planar.

A theoretical calculation of the structure and the vibrational frequencies of $CuCH_2$ has been carried out. Assuming C_{2v} symmetry, a minimum basis set was used in the UHF calculation without any correlation of the electrons. The SCF optimized $CuCH_2$ molecular geometry is shown below:

$r_1 = r_2 = r(C\text{-}H) = 1.079$ Å

$r_3 = r(Cu\text{-}C) = 1.81$ Å

$\phi_1 = \phi_2 = \angle(CuCH) = 123.11°$

$\phi_3 = \angle(CH_2) = 113.78°$

$\theta_1 = 180.0°$

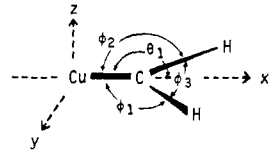

The calculated parameters are similar to those calculated for $NiCH_2$[10] where r(Ni–C) = 1.78 Å, r(C–H) = 1.071 Å, and ∠(CH_2) = 113°. If we assume that the methylene moiety can be treated independently as a triatomic molecule, then a ∠(CH_2) bond angle of 113°[11] is calculated from the CH_2 s-stretching, a-stretching, and CH_2 bending frequencies of $CuCH_2$, $Cu^{13}CH_2$, and $CuCD_2$.[12] These values can be compared to 107 (9)° in

Scheme I

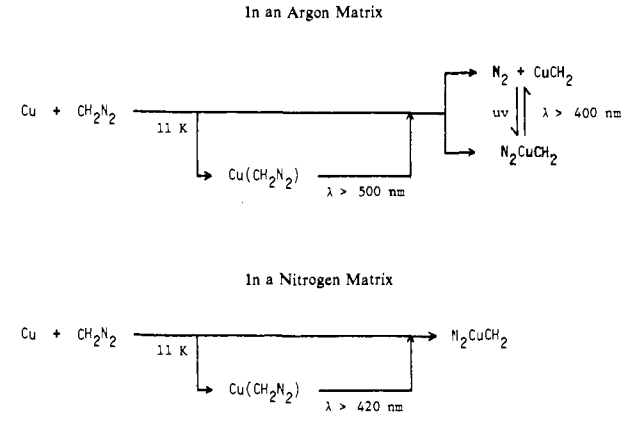

$Ta(\eta_5\text{-}C_5H_5)_2(CH_3)(CH_2)$.[13] The theoretical estimated vibrational frequencies for $CuCH_2$ are 528 (CH_2 wag), 617 (CuC stretch), 700 (CH_2 rock), 1589 (CH_2 scissor), 3640 (CH_2 s-stretch), and 3776 (CH_2 a-stretch) cm^{-1}. Although the CH_2 stretching frequencies appear very high, the calculated frequencies for Cu–C stretching and CH_2 wagging are in good agreement with observed values.

The theoretically determined geometric parameters were used in the normal coordinate analyses for $CuCH_2$, N_2CuCH_2, and their isotopic molecules, as shown in Tables I and II. A derived set of force constants for $CuCH_2$ from the analysis is listed in Table IV.

Conclusion

The overall reaction pattern of copper atoms with diazomethane in cryogenic matrices is shown in Scheme I. The reactions can be summarized as follows. The insertion of copper atoms into the NC bond of diazomethane occurs in part spontaneously during the cocondensation process on the matrix surface. The insertion products are isolated and characterized as $CuCH_2$ and N_2CuCH_2 ($CuCH_2/N_2CuCH_2 \simeq 4/1$). These two species can be photolytically interconverted in argon matrices. In nitrogen matrices only N_2CuCH_2 is isolated and the coordinated N_2 group cannot be photodissociated. Copper diazomethane adducts, $Cu(CH_2N_2)$, are also formed and isolated in both argon and nitrogen matrices upon deposition. The copper–diazomethane adducts can be

(11) Unpublished results.
(12) (a) Allavena, M.; Rysnik, R.; White, D.; Calder, V.; Mann, D. E. *J. Chem. Phys.* **1969**, *50*, 3399. (b) Green, D. W.; Ervin, K. M. *J. Mol. Spectrosc.* **1981**, *88*, 51.
(13) Guggenberger, L. J.; Schrock, R. R. *J. Am. Chem. Soc.* **1975**, *97*, 6577.
(14) Moore, C. B.; Pimentel, G. C. *J. Chem. Phys.* **1964**, *40*, 342.

photoexcited, and metal atom insertion into the CN bond of the adducted diazomethane occurs. Finally, it would be of interest to compare the force constants of the CuC stretch in $CuCH_2$ and $CuCH_3$; however, some uncertainty exists with respect to the assigned CuC stretching mode for $CuCH_3$.[8] When this value is available it will be possible to assess the degree of double-bond character in the Cu–C bond of $CuCH_2$.

Acknowledgment. The financial support of the National Science Foundation, the Robert A. Welch Foundation, and the 3M Company are greatly appreciated. We gratefully acknowledge the assistance of Tom A. Holme with the UHF calculations of $CuCH_2$.

Registry No. $CuCH_2$, 108295-75-6; $Cu^{13}CH_2$, 108295-76-7; CuCHD, 108295-77-8; $CuCD_2$, 108295-78-9; N_2CuCH_2, 108295-79-0; $N_2Cu^{13}CH_2$, 108295-80-3; N_2CuCHD, 108295-81-4; N_2CuCD_2, 108295-82-5; Cu, 7440-50-8; N_2CH_2, 334-88-3; Ar, 7440-37-1; N_2, 7727-37-9.

Solid-State ^{31}P NMR Studies of DNA Liquid Crystalline Phases. The Isotropic to Cholesteric Transition†

Teresa E. Strzelecka and Randolph L. Rill*

Contribution from the Department of Chemistry and Institute of Molecular Biophysics, Florida State University, Tallahassee, Florida 32306. *Received December 11, 1986*

Abstract: Aqueous solutions of short DNA fragments with Na^+ as counterion form a cholesteric liquid crystalline phase when the DNA concentration exceeds a critical value dependent on DNA length and solution ionic strength. Transitions of solutions of 146 base pair (ca. 500-Å) length DNA between cholesteric and isotropic phases were monitored by ^{31}P solid-state NMR spectroscopy and polarizing microscopy. Isotropic phase formation upon increase of temperature or decrease of DNA concentration was indicated by the appearance of a sharp isotropic resonance superimposed on a broad resonance of the anisotropic phase. A phase diagram for transitions between isotropic and cholesteric phases in buffered DNA solutions with a sodium ion activity of 0.21 M was calculated from integrated areas of the isotropic and cholesteric phase resonances. The phase diagram is in good agreement with that predicted by the lattice statistics treatment of phase equilibria in solutions of weakly interacting, nonelectrolyte, rodlike particles by Flory. The fully isotropic and cholesteric phase boundaries are only weakly dependent on temperature and are separated by a narrow biphasic region in which the two phases coexist. At 20 °C the solutions were biphasic at DNA concentrations from 125 to 155 mg/mL and fully liquid crystalline above 155 mg/mL. The observed DNA phase boundaries agreed well with Flory's theory of noninteracting rods assuming a best-fit effective DNA radius of 21.5 ± 1 Å, in good agreement with the effective DNA radius determined at approximately this ionic strength by other methods employing scaled particle theory. This agreement suggests that isotropic to liquid crystalline phase transitions of semirigid polyelectrolytes modeled as scaled particles can be treated to a good first approximation in terms of Flory's theory. Preliminary evidence for a higher order DNA phase is also presented.

DNA concentrations in vivo range from a few milligrams per milliliter in eukaryotic chromatin to over 70% in phage and sperm heads; hence understanding of mechanisms of DNA packing in vivo requires knowledge of the behavior of highly concentrated DNA solutions. As first described by Onsager[1] and elaborated by Flory and others,[2] rodlike and semirigid polymers are expected to form ordered, liquid crystalline-like phases above some critical volume fraction due to the dominance of excluded volume effects. This behavior has been well documented for synthetic, nonelectrolyte polymers,[3] but not for polyelectrolytes. DNA and other semirigid, polyelectrolyte biopolymers are expected to order analogously to uncharged polymers due to the same dominance of excluded volume effects. The necessity for counterion screening of the high charge density on DNA introduces a complicating factor, however, since the condensed counterion atmosphere will contribute to the effective particle radius and hence to the effective axial ratio and volume fraction.[4]

Recent studies have shown that short DNA fragments in vitro in aqueous solutions with K^+, Na^+, or Mg^{2+} as supporting counterion can exist in at least two different condensed or aggregated phases depending on DNA concentration, ionic strength, and temperature. A gel-like phase occurs in solutions of Na^+ DNA and Mg^{2+} DNA with concentrations up to 35 mg/mL.[5] More concentrated DNA solutions form phases with cholesteric-like liquid crystalline order.[4a,6] Cholesteric-like organization has also been observed in solutions of high molecular weight DNA and in chromosomes of lower organisms such as dinoflagellates.[7] Evaluation of mechanisms leading to spontaneous cholesteric ordering of DNA is therefore important for understanding DNA condensation in vivo and the more general behavior of solutions of semirigid polyelectrolytes.

We have used solid-state ^{31}P NMR methods to obtain the first quantitative phase diagram for the isotropic to cholesteric tran-

†This work was supported in part by grants from the Department of Energy (EV05888) and the National Institutes of Health (GM37098).

*To whom reprint requests should be addressed at the Department of Chemistry.

(1) Onsager, L. *Annu. Rev. Biochim.* **1949**, *51*, 627–659.
(2) (a) Flory, P. J. *Proc. R. Soc. London, Ser. A* **1956**, *234*, 60–73, 73–89. (b) Flory, P. J. In *Polymer Liquid Crystals*; Ciferri, A., Krigbaum, W. R., Meyer, R. B., Eds.; Academic: New York, 1982; pp 103–112 and references cited therein. (c) Lasher, G. *J. Chem. Phys.* **1970**, *53*, 4141–4146.
(3) (a) Robinson, C. *Trans. Faraday Soc.* **1956**, *52*, 571–592; also *Faraday Soc. Discuss.* **1958**, *25*, 29–41. (b) Miller, W. *Annu. Rev. Phys. Chem.* **1979**, *29*, 219 and references cited therein.
(4) (a) Brian, A. A.; Frisch, H. L.; Lerman, L. S. *Biopolymers* **1981**, *20*, 1305–1328. (b) Stigter, D. *Biopolymers* **1977**, *16*, 1435–1448; also *J. Phys. Chem.* **1978**, *82*, 1603–1606. (c) Record, T. M.; Anderson, C. F.; Lohman, T. M. *Q. Rev. Biophys.* **1978**, *11*, 1–3–178. (d) Le Bret, M.; Zimm, B. H. *Biopolymers* **1984**, *23*, 271–285, 286–312.
(5) Fried, M. G.; Bloomfield, V. A. *Biopolymers* **1984**, *23*, 2141–2155.
(6) (a) Rill, R. L.; Hilliard, P. R., Jr.; Levy, G. C. *J. Biol. Chem.* **1983**, *258*, 250–256. (b) Rill, R. L. *Proc. Natl. Acad. Sci. U.S.A.* **1986**, *83*, 342–346. (c) Brandes, R.; Kearns, D. R. *Biochemistry* **1986**, *25*, 5890–5895.
(7) (a) Robinson, C. *Tetrahedron* **1961**, *13*, 219. (b) Luzzati, V.; Nicolaieff, A.; Masson, F. *J. Mol. Biol.* **1961**, *3*, 185–201. (c) Maniatis, T.; Venable, J. H.; Lerman, L. S. *J. Mol. Biol.* **1974**, *84*, 37–64. (d) Iizuka, E. *Polym. J.* **1977**, *9*, 173–180; also *10*, 235–237, 293–300. (e) Iizuka, E.; Kondo, Y. *Mol. Cryst. Liq. Cryst.* **1979**, *51*, 285–294. (f) Livolant, F. *Eur. J. Cell Biol.* **1984**, *33*, 300–311.

0002-7863/87/1509-4513$01.50/0